ADVANCED FUNCTIONAL MATERIALS
www.afm-journal.de



# Electrochemical and Top-Down 3D Ion-Carving to Change Magnetic Properties

*Jian Zhu and Da Deng**

**It is challenging to develop new top-down approaches to tailor particles into subnanometer size structures on a large scale to further reveal their structure-dependent physicochemical properties. Here, we demonstrate a non-conventional, electrochemical, 3D ion-carving process to tailor particles into subscale flower-like nanostructures at room temperature. The technology is based on the electrochemical insertion/extraction of lithium ions as a carving "knife" to carve the single-crystalline particle precursor into higher-order, flower-like nanostructures with hexagonal nanopetals as the building units. Our study demonstrates that the morphology of the as-carved, flower-like nanostructures can be controlled by the electrochemical parameters, such as the current density and the number of cycles. Particularly interesting is that dramatically different magnetic properties can be achieved depending on the morphology through careful tuning by the electrochemical ion-carving process. The as-carved, flower-like particles may find many important applications, including magnetic nanodevices. Our approach, in principle, is applicable to prepare various kinds of 3D-structured materials with different compositions.**

## 1. Introduction

Innovative methods to carve micro- and nanosized particles into unique subscale nanostructures and tune their structure-dependent functional properties are highly desirable technologies. However, such technologies are challenging to develop. Nanostructured materials with an engineered morphology and unique physicochemical properties have been attracting significant attention over the past decades. Nanostructured materials can find important applications in many fields, such as catalysis,[1] energy conversion and storage,[2] sensors,[3] electronics,[4] and biomedical applications.[5] It is still a challenging task to find a facile synthesis of nanostructures with designed structures and/or orientation, particularly, for preparation on a large scale. There are two general approaches to preparing nanostructured materials, namely, top-down and bottom-up methods. Many bottom-up techniques have been explored to make nanostructured materials, including template-assisted,[6] solvothermal,[7] microwave-assisted,[8] sol-gel,[9] and chemical/physical vapor deposition methods.[10] On the other hand, few techniques are available for the top-down creation of nanostructures, which is particularly difficult for mass production. Generally, the top-down methods are limited to mechanical milling,[11] chemical etching,[12] photolithography, and electron-beam lithography.[13] Those top-down techniques usually suffer from poor morphology control and/or difficulties for large-scale production. Electrochemical machining (ECM) has been employed for machining extremely hard materials in bulk for over fifty years and ECM is popularly used to make gas turbine blades. It will be interesting to explore electrochemical nanomachining (ECNM) as a top-down technique to manipulate and carve particles with a simple morphology into nanostructures with higher-order complex structures at the nanoscale. Electrochemical milling processes have been employed to create nanoporous Pt, $RuO_2$, Ge, and Cu nanoparticles by conversion or alloying reactions.[14] The electrochemical milling technique, arguably, could be considered a passive and destructive top-down approach that makes it difficult to form higher-order nanostructures. Electrochemically induced exfoliation by Li-ion insertion has also been applied to make 2D nanomaterials from layered transition-metal dichalocogenides, metal oxides, hexagonal boron nitride, and graphite.[15] It should therefore be interesting to develop an electrochemical carving process as a top-down approach to tailor and create nanostructures from simple precursor particles. Recently, we have successfully demonstrated that electrochemical sodium-ion insertion could be used as a top-down approach to cut carbon nanospheres into two bowl-like hemispheres on a large scale.[16] We wanted to expand and develop this method into a general electrochemical ion-carving technology or ECNM for the top-down tailoring of other nanoparticles, including metal oxides.

Herein, we report a facile, top-down, electrochemical ion-carving approach based on ECNM to facilely carve simple rhombohedral $\alpha$-$Fe_2O_3$ particles into hierarchical flower-like nanostructures composed of nanoflakes as the building units. We found that the electrochemical parameters, including the testing current and number of lithiation–delithiation cycles could be used to tune and control the morphology of the final

J. Zhu, Prof. D. Deng
Department of Chemical Engineering
and Materials Science
Wayne State University
5050 Anthony Wayne Drive, Detroit, MI 48202, USA
E-mail: da.deng@wayne.edu

DOI: 10.1002/adfm.201502916

carved nanostructures. We demonstrate that a common phenomenon of electrochemical conversion reactions, which are commonly observed in lithium-ion batteries, can be turned into a general electrochemical carving technology for the top-down creation of nanostructures from precursor particles. Additionally, the as-carved, battery-derived, flower-like, $\alpha$-$Fe_2O_3$ nanostructures revealed interesting, electrochemically tunable, magnetic properties. We believe that the idea outlined in this paper will be interesting to the fields of rechargeable batteries, nanomaterials fabrication, battery-derived materials and magnetism.

## 2. Results and Discussion

The morphology of the precursor rhombohedral $\alpha$-$Fe_2O_3$ particles[17] was revealed by field-emission scanning electron microscopy (FESEM) images (**Figure 1**a,b), which can be compared with those of the as-carved flower-like nanostructures (Figure 1c–f). The low-magnification FESEM image in Figure 1a shows the microscale rhombohedral structure of the as-prepared $\alpha$-$Fe_2O_3$ precursor with good size distribution. The size of the precursor was around 800 nm. The high-magnified FESEM image in Figure 1b shows several representative microscale $\alpha$-$Fe_2O_3$ rhombohedra, which clearly reveals the surface texture of the particles with smooth exteriors and clean edge outlines. The success of the electrochemical ion-carving method to convert the precursor rhombohedral $\alpha$-$Fe_2O_3$ particles into flower-like $\alpha$-$Fe_2O_3$ nanostructures is revealed by the FESEM images in Figure 1c–f. The uniform conversion from rhombohedral particles to flower-like nanostructures is revealed in the low-magnification FESEM image (Figure 1c), where all the rhombohedra were converted into nanoflowers composed of nanoflakes as the building units. The highly rough texture of those aggregated flower-like nanostructures suggested that the smooth exterior of the precursor rhombohedra were carved into highly rough structures (Figure 1d). Close examination revealed that not all the particles were carved to the same degree, which could be related to the morphology of an intermediate compound at the early stage of ion carving. The nanoscale details of the as-carved, flower-like, $\alpha$-$Fe_2O_3$ nanostructures are revealed in the high-magnification FESEM image in Figure 1e. In contrast to their precursor shown in Figure 1b, the surface of the as-carved, flower-like nanostructure was covered with intercrossed nanoflakes or nanopetals. Intercrossed nanopetals endow the structure with a larger exposed surface area as compared to its precursors, which is preferable for certain applications, such as catalysis. More details about the building units of the nanopetals were revealed by additional high-magnification views of a typical structure with less intercrossed nanopetals (Figure 1f). The thickness of the nanopetals here was between 20 and 33 nm. Interestingly, the 2D nanopetals had a hexagonal shape with an edge length of about 350 nm. Several half-hexagonal or trapezoid petals also grew on the surface of the hexagonal nanopetals because of intercrossing. The EDS results of the as-carved flower-like nanostructures were compared to their precursor (Figure S1 and S2 in the Supporting Information). The ratio of Fe/O was almost identical for both the as-derived nanoflowers and their precursor, which suggests that they might have the same chemical composition. The electrochemical reactions involved are highly reversible in terms of leading to the same chemical composition, but they could dramatically change the morphology resulting in the carved particles.

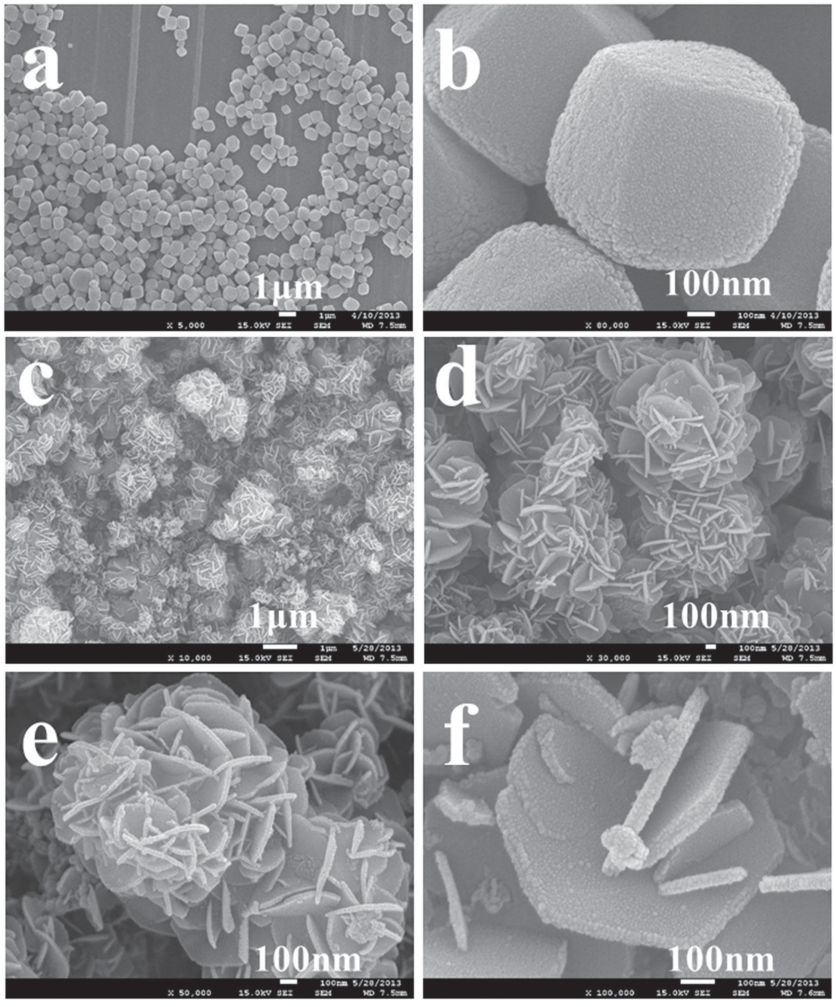


**Figure 1.** FESEM images of: a,b) the precursor rhombohedral $\alpha$-$Fe_2O_3$ particles at a) low-magnification and b) a representative view at high magnification;[17] c–f) the as-carved battery-derived flower-like $\alpha$-$Fe_2O_3$ nanostructures derived from the precursor particles: c) low-magnification image to show that all the precursor particles were electrochemically carved into flower-like hierarchical nanostructures; d) zoom-in to show a few representative flower-like structures that have aggregated; e) a typical $\alpha$-$Fe_2O_3$ flower with nanopetals; f) magnified image of intercrossed nanopetals with hexagonal shape. Number of cycles: 120.

The as-carved flower-like $\alpha$-$Fe_2O_3$ was further investigated by transmission electron microscopy (TEM) (**Figure 2**). A

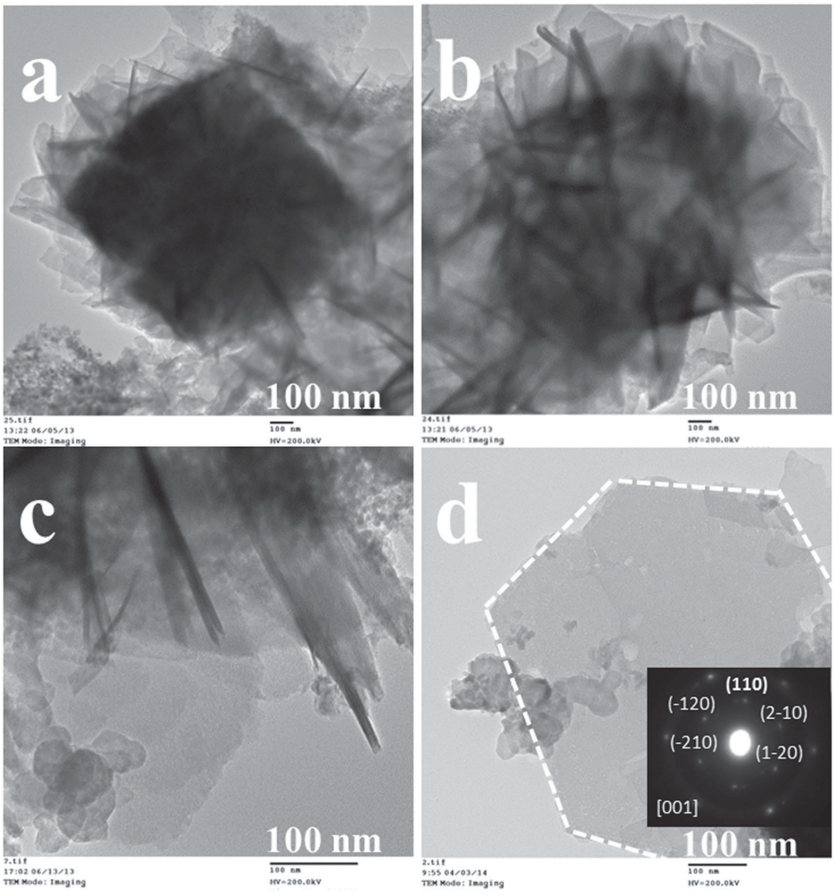


**Figure 2.** The as-carved flower-like $\alpha$-$Fe_2O_3$ nanostructures characterized by TEM: a) a representative particle with intercrossed nanopetals on the surface of the rhombohedron indicating the early stage of carving, b) a particle with the core part of the precursor rhombohedron formed by aggregated nanoflakes indicating a fully carved stage, c) high-magnification image showing a few nanopetals from different perspectives confirming their 2D nature, and d) a single piece of hexagonal nanopetal with the outline highlighted. The inset of (d) is the SAED pattern. Number of cycles: 120.

typical $\alpha$-$Fe_2O_3$ flower with intercrossed nanopetals is shown in Figure 2a. All the intercrossed nanopetals had grown outward from the surface of the rhombohedral core and the core was fully covered by those intercrossed nanopetals. The outline of the rhombohedral core is clearly visible as a dark shadow, indicating the early stage of carving. Figure 2b shows another typical image where the precursor rhombohedron was probably fully carved, indicated by the fact that the $\alpha$-$Fe_2O_3$ flower at the core was fully contrasted in light. A high-magnification view of a few intercrossed nanopetals, whereby each of the nanopetals is oriented at different degrees, suggests that the nanopetals are 2D structures, such as nanoflakes (Figure 2c). A piece of detached nanopetal/nanoflake clearly shows the typical hexagonal shape (Figure 2d). High-resolution TEM (HRTEM) was used to analyze the lattice fringes of the hexagonal nanopetal (Figure S3 in the Supporting Information). The interplanar spacing of 0.25 nm can be assigned to the (110) plane of $\alpha$-$Fe_2O_3$. Furthermore, the selected-area electron diffraction (SAED) pattern (inset of Figure 2d) can be assigned to crystalline $\alpha$-$Fe_2O_3$ with the electron beam in the [001] direction.[18] The nanopetals were estimated to have about 90% of exposed hexagonal {001} facets, in contrast to their precursor rhombohedral particles with dominantly exposed {104} facets. Based on both HRTEM and SAED analysis, we can conclude that the nanopetals are crystalline $\alpha$-$Fe_2O_3$.

The chemical composition of the as-carved particles was further confirmed by X-ray photoelectron spectroscopy (XPS) (**Figure 3**). Figure 3a shows the O 1s XPS spectrum, where the peaks at 532.2, 531.1, and 529.6 eV can be assigned to the surface hydroxyls (Fe-OH), the C–O–Fe bond, and the lattice oxygen in hematite (Fe-O in $Fe_2O_3$), respectively.[19] The Fe 2p photoelectron peaks appeared around 724.4 and 711.1 eV, which can be assigned to Fe 2p 1/2 and Fe 2p 3/2, respectively. Both peaks agreed well with previously reported values in the literature, indicating the existence of $Fe^{3+}$.[20] The characteristic satellite peak for $Fe^{3+}$ species was observed at around 718.1eV. These three main peaks were in good agreement with those of $\alpha$-$Fe_2O_3$.[20a,21] Moreover, the absence of the Fe 2p 3/2 peak of $Fe^0$ at around 706.8 eV indicates that the intermediate metallic Fe was converted back to $Fe_2O_3$ through a reversible electrochemical reaction. Therefore, the experimental results from XPS, EDS, HRTEM, and SAED analysis all clearly evidenced that the as-carved flower-like particles are dominantly $Fe_2O_3$, which could be attributed to the reversible electrochemical reactions involved. No impurities or intermediate components were detected, which indicates that their presence, if any, was very small.

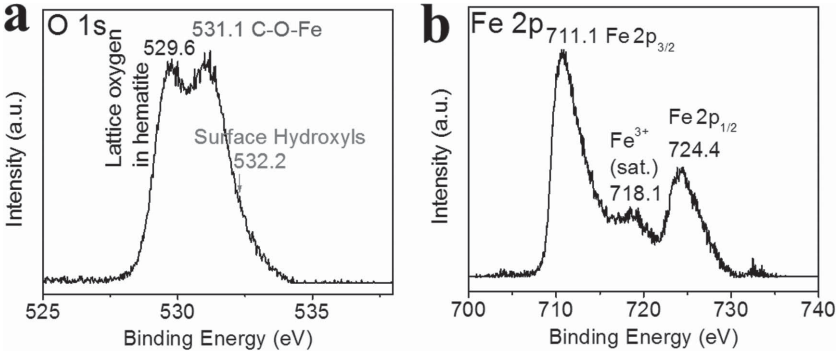


**Figure 3.** XPS of as-carved flower-like $\alpha$-$Fe_2O_3$: a) O 1s narrow scan spectrum and b) Fe 2p narrow scan spectrum.

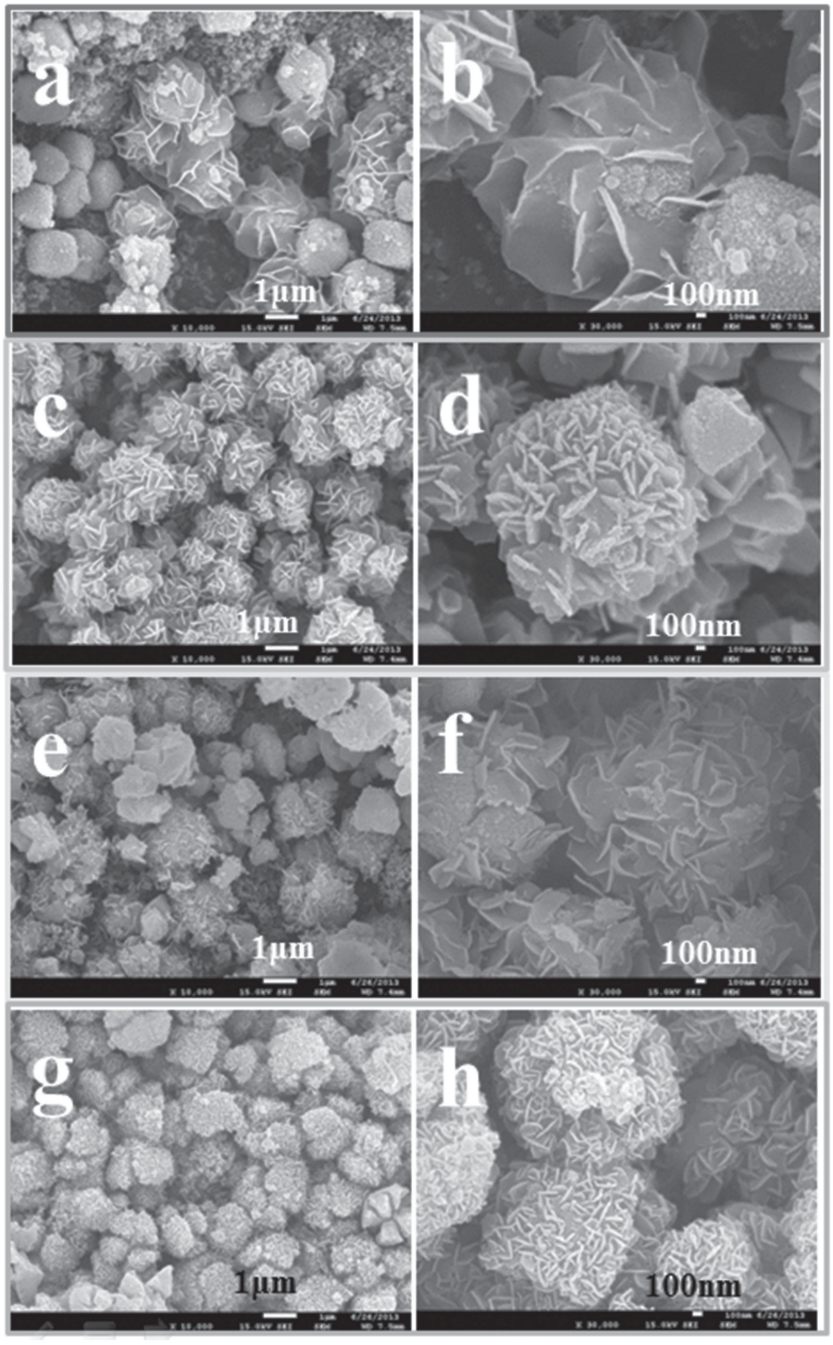


**Figure 4.** FESEM images of $\alpha$-$Fe_2O_3$ with flowerlike structure that had been electrochemically carved at different currents of a,b) 100; c,d) 200; e,f) 400; and g,h) 800 mA $g^{-1}$, at low (a,e,g) and high (b,f,h) magnification. Number of cycles: 10.

We found that the applied current could significantly affect the morphology of the carved structures. The morphologies of as-carved flower-like $\alpha$-$Fe_2O_3$ structures under different electrochemical currents are shown in **Figure 4**. At a current density of 100 mA $g^{-1}$ for 10 cycles, some rhombohedra were covered by irregular nanoparticles, and another portion of the particles had flower-like structures (Figure 4a,b). The thin and curved nanopetals covering the surface of the rhombohedra were not flat polygonal shapes. When the current density was increased, the flower-like structures were universally observed on all surfaces. At a current density of 200 mA $g^{-1}$, the nanopetals covered the surface of all rhombohedra, and an early stage of carving could be seen on the surface of the precursor (Figure 4c,d). Compared to this, we created the same carved flower-like structures at the same current but for 120 cycles and found that prolonging the reaction time or increasing the number of cycles also offered a deeper degree of carving. The well-defined flower-like structures after either 10 or 120 cycles suggest that the battery-derived flower-like structures were highly stable under the ECNM conditions. At higher current densities of 400 or 800 mA $g^{-1}$ the nanopetals appeared more densely on the surface of the precursor rhombohedra (Figure 4e-h). We also observed some cracks on a few of the carved rhombohedra, which could be attributed to the huge volume variation in the short period of time of lithium ion insertion, or the "force" used to carve was too high.

The electrochemical reduction–oxidization profiles, corresponding to the charge–discharge profiles, of the precursor rhombohedra carved at different current densities were analyzed. **Figure 5** shows a typical profile cycled at a current of 200 mAh $g^{-1}$. Additional profiles cycled at various current densities are shown in Figure S4 in the Supporting Information. The highly similar profiles suggest that the electrochemical reactions involved were the same under all different current densities, as expected. The plateau for the first reduction cycle around 0.7 V, which shifted to around 1.0 V from the second reduction cycle onwards, could be attributed to the reduction of $Fe_2O_3$ to $Fe^0$ and the formation of $Li_2O$. The plateau around 1.5–1.7 V could be attributed to the reverse oxidization reaction. The overall electrochemical reaction could then be: $Fe_2O_3 + 6\ Li^+ + 6e^- \leftrightarrow 2Fe^0 + 3Li_2O$.[3,21a,22] The $dQ/dV$ vs. $V$ curves also confirmed the electrochemical reactions involved (Figure S5 in the Supporting Information).

We propose the following mechanism to explain the electrochemical ion-carving process (**Figure 6**), for which the reversible electrochemical reactions involved have been well documented before:[23]

$$\alpha\text{-}Fe_2O_3 + Li^+ + e^- \leftrightarrow \alpha\text{-}LiFe_2O_3 \quad (1)$$

$$\alpha\text{-}LiFe_2O_3 + Li^+ + e^- \leftrightarrow Li_2Fe_2O_3 \quad (2)$$

$$Li_2Fe_2O_3 + 4Li^+ + 4e^- \leftrightarrow 2Fe^0 + 3Li_2O \quad (3)$$

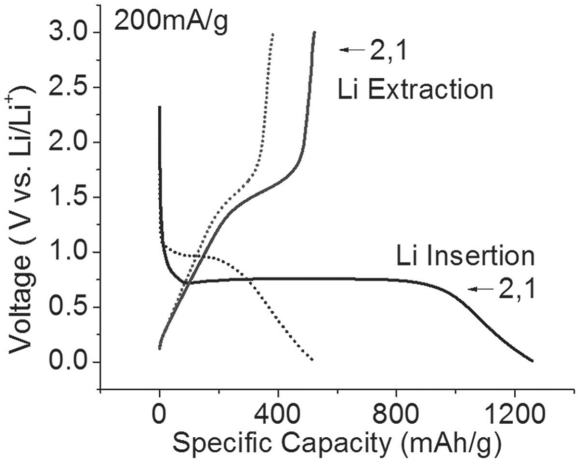


**Figure 5.** A typical electrochemical lithium reduction–oxidization profile for the first two cycles at a current of 200 mA $g^{-1}$.

Upon electrochemical reduction, an $Fe^0$ nanoparticle will be formed and will be embedded in the amorphous $Li_2O$ matrix that is simultaneously formed.[24] The electrochemical lithium insertion process will cause a volume expansion, which leads to a high stress at the interface. At the same time, $Li_2O$ is not conductive; so the $Fe^0$ nanoparticles may arrange in such a way as to alleviate the stress at the reaction interface, and at the same time maintain the electron conducting paths that enable further reduction towards the core part. The creation and migration of dislocations might also occur at the interface under stress. Upon oxidization, the arranged $Fe^0$ could be oxidized back to $Fe_2O_3$ thus forming the nanopetals. The electrochemical carving process is repeated upon additional number of cycles

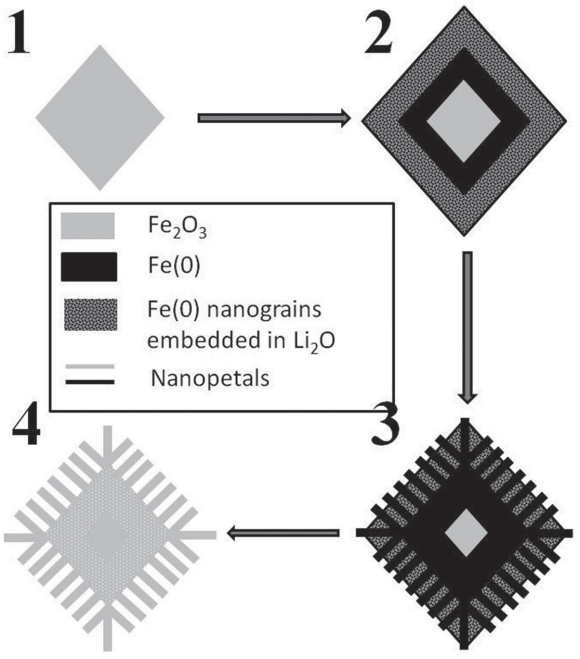


**Figure 6.** Schematic of the proposed mechanism for the electrochemical ion-carving process.

to form intercrossed nanopetals in the form of nanoflower-like structures. We believe our ion-carving technology is an active approach to the top-down tailoring of particles, which could be considered as an alternative way to utilize electrochemical pulverization that is commonly observed in batteries. Here, we have successfully demonstrated that this technology may enable the carving of rhombohedra into substructures of 2D nanopetal aggregates, using $Fe_2O_3$ as an example. We believe that this top-down, electrochemical ion-carving approach, which has been preliminarily demonstrated here, can be extended to prepare other materials with various ions or ECNM to make battery-derived nanostructures. However, additional work is required to better understand the mechanism.

The as-carved flower-like $\alpha$-$Fe_2O_3$ particles demonstrated interesting magnetic properties that are significantly different from that of their precursors (**Figure 7**). It is well known that magnetic properties in general can significantly be affected by the shape and size of the compound at the nanoscale.[25] The magnetic hysteresis loops of the microsized rhombohedral precursor and that of the flower-like materials indicate the existence of $\alpha$-$Fe_2O_3$ with ferromagnetic behavior.[20b,d,26] The remnant magnetization ($M_r$) and coercivity force ($H_c$) were 0.230 emu $g^{-1}$ and 6.1 kOe for the precursor $\alpha$-$Fe_2O_3$ rhombohedra (Figure 7a). In comparison, the $M_r$ and $H_c$ were 0.062 emu $g^{-1}$ and 18.0 Oe for flower-like $\alpha$-$Fe_2O_3$ structures that had been electrochemically carved after 10 cycles (Figure 7c). After 120 cycles the flower-like $\alpha$-$Fe_2O_3$ structures attained an $M_r$ and $H_c$ of 0.790 emu $g^{-1}$ and 71.0 Oe (Figure 7b). The different $M_r$ and $H_c$ observed for the flower-like nanostructures could be ascribed to the changes in anisotropy of the particles.[26c] The differences in the remnant magnetization and coercivity observed suggest that the magnetic properties could also be tuned by choosing to perform the electrochemical carving at different degrees. Further work should be carried out to thoroughly explore the relationship between the morphology induced by the electrochemical carving and the magnetic properties. We believe that the as-carved flower-like $Fe_2O_3$ may find many other applications, including batteries, catalysis, optical and magnetic devices, as well as model materials for the investigation of surface properties.

## 3. Conclusion

A non-conventional, top-down approach, namely electrochemical ion-carving or ECNM, was demonstrated to create flower-like $\alpha$-$Fe_2O_3$ nanostructures from precursor rhombohedra. The influence of the current density and the number of cycles on the carved morphology were investigated. We have shown that the electrochemical parameters could be used to tune the final morphology. Interestingly, their magnetic properties could also be tuned. We believe that this technology could be highly effective for the room-temperature tailoring of nanoparticles into substructures on a large scale and to further reveal their structure-dependent properties, including their catalytic, magnetic, and optical properties. The idea outlined in this paper will be tested for different materials (oxides, sulfides, nitrides, carbides, metals, etc.) using various ions ($Li^+$, $Na^+$, $Mg^{2+}$, $K^+$, $Ca^{2+}$, $Al^{3+}$, etc.), and the results will be reported once available.

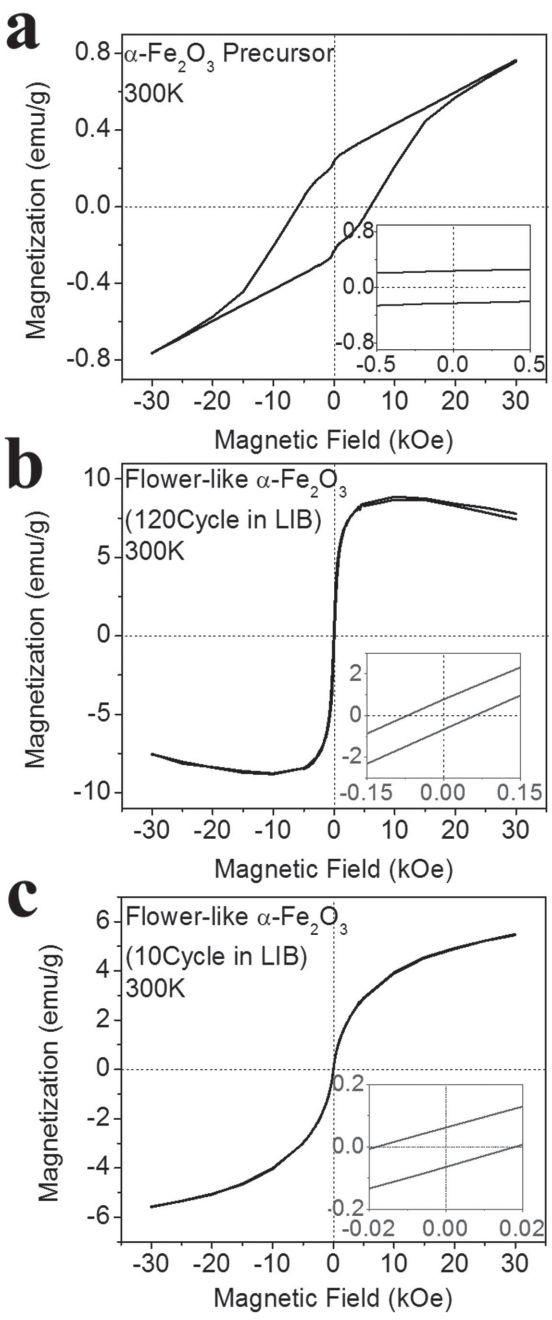


**Figure 7.** Magnetization versus applied magnetic field dependence recorded at 300 K: a) precursor $\alpha$-$Fe_2O_3$ rhombohedra, b) as-carved flowerlike $\alpha$-$Fe_2O_3$ after 120 cycles, and c) as-carved flowerlike $\alpha$-$Fe_2O_3$ after carving for 10 cycles at a current of 200 mA $g^{-1}$. The insets are the corresponding magnifications.

## 4. Experimental Section

*Electrochemical Ion-Carving*: The precursor rhombohedral $\alpha$-$Fe_2O_3$ particles with sizes around 800 nm were prepared following a previously reported procedure.[17] For the electrochemical ion-carving ECNM treatment, the as-prepared rhombohedral $\alpha$-$Fe_2O_3$ particles were first mixed with a carbon conductivity enhancer (Super-P carbon black, Timcal), and a polyvinylidene fluoride binder in the weight ratios of 80:10:10 in a *N*-methylpyrrolidon solvent. The slurry was cast on copper discs and dried in a vacuum oven at 100 °C overnight. Typically, the as-coated copper disc was used as the working electrode, metallic Li foil as the counter and reference electrode, and a 1 M solution of LiPF6 in a 50:50 v/v mixture of ethylene carbonate and diethyl carbonate (DEC) was used as the electrolyte and all of these were assembled into a cell. The rhombohedral $\alpha$-$Fe_2O_3$ particles were carved electrochemically at room temperature in the voltage window of 0.01 V–3 V at a current of 200 mA $g^{-1}$ for various numbers of cycles (e.g., 10 or 120 cycles) on a MTI BST8-WA battery tester.[17] The as-carved flower-like $\alpha$-$Fe_2O_3$ nanostructures were collected by disassembling the cell and washing with water and ethanol for multiple times, followed by additional washing with DEC for three times to remove the soluble Li salts and other organic residues. The flower-like $\alpha$-$Fe_2O_3$ nanostructures were further washed with ethanol for several times and dried in vacuum at room temperature overnight.

*Materials Characterization*: The as-carved, flower-like $\alpha$-$Fe_2O_3$ nanostructures were characterized by field-emission scanning electron microscopy (JSM-7600, FE-SEM, equipped with a Pegasus Apex 2 integrated EDS) and transmission electron microscopy (JEOL 2010 TEM). X-ray photoelectron spectroscopy (XPS) analysis was performed using a Perkin Elmer ESCA 5500 instrument with Al K$\alpha$ radiation (15 kv, 15mA, 210Watts). Their magnetic properties were tested at 300 K from –30 kOe to 30 kOe on a physical property measurement system (PPMS, Quantum Design Model 6000).

## Supporting Information

Supporting Information is available from the Wiley Online Library or from the author.

## Acknowledgements

We thank Guangzhao Mao for access to XRD, Gregory Auner for access to XPS, Gavin Lawes for access to PPMS, and the Lumigen Instrument Center for access to FESEM and TEM.

Received: July 14, 2015
Revised: August 15, 2015
Published online: September 15, 2015

[1] Z. Zhang, H. Che, Y. Wang, X. She, J. Sun, P. Gunawan, Z. Zhong, F. Su, *ACS Appl. Mater. Interfaces* **2012**, *4*, 1295.
[2] a) G. Zhang, L. Yu, H. B. Wu, H. E. Hoster, X. W. Lou, *Adv. Mater.* **2012**, *24*, 4609; b) L. Zhou, D. Zhao, X. W. Lou, *Adv. Mater.* **2012**, *24*, 745.
[3] J. Chen, L. Xu, W. Li, X. Gou, *Adv. Mater.* **2005**, *17*, 582.
[4] S.-W. Hwang, *Nano Lett.* **2015**, *15*, 2801.
[5] S. J. Son, J. Reichel, B. He, M. Schuchman, S. B. Lee, *J. Am. Chem. Soc.* **2005**, *127*, 7316.
[6] X. Xu, R. Cao, S. Jeong, J. Cho, *Nano Lett.* **2012**, *12*, 4988.
[7] a) J. Lian, X. Duan, J. Ma, P. Peng, T. Kim, W. Zheng, *ACS Nano* **2009**, *3*, 3749; b) C.-Y. Cao, J. Qu, W.-S. Yan, J.-F. Zhu, Z.-Y. Wu, W.-G. Song, *Langmuir* **2012**, *28*, 4573.
[8] a) X. Hu, J. C. Yu, J. Gong, Q. Li, G. Li, *Adv. Mater.* **2007**, *19*, 2324; b) Z. Ai, K. Deng, Q. Wan, L. Zhang, S. Lee, *J. Phys. Chem. C* **2010**, *114*, 6237.
[9] a) R. Sui, P. Charpentier, *Chem. Rev.* **2012**, *112*, 3057; b) Y. Kido, K. Nakanishi, A. Miyasaka, K. Kanamori, *Chem. Mater.* **2012**, *24*, 2071.
[10] a) S. C. Sahoo, D. R. Mohapatra, H.-J. Lee, S. M. Jejurikar, I. Kim, S.-C. Lee, J.-K. Park, Y.-J. Baik, W.-S. Lee, *Carbon* **2014**, *67*, 704; b) P. A. Pandey, G. R. Bell, J. P. Rourke, A. M. Sanchez, M. D. Elkin, B. J. Hickey, N. R. Wilson, *Small* **2011**, *7*, 3202.

[11] J. Hassoun, G. Mulas, S. Panero, B. Scrosati, *Electrochem. Commun.* **2007**, *9*, 2075.
[12] J. S. Chen, T. Zhu, X. H. Yang, H. G. Yang, X. W. Lou, *J. Am. Chem. Soc.* **2010**, *132*, 13162.
[13] a) S. Sun, G. J. Leggett, *Nano Lett.* **2004**, *4*, 1381; b) R. Near, C. Tabor, J. Duan, R. Pachter, M. El-Sayed, *Nano Lett.* **2012**, *12*, 2158.
[14] a) Y.-S. Hu, Y.-G. Guo, W. Sigle, S. Hore, P. Balaya, J. Maier, *Nat. Mater.* **2006**, *5*, 713; b) X. H. Liu, S. Huang, S. T. Picraux, J. Li, T. Zhu, J. Y. Huang, *Nano Lett.* **2011**, *11*, 3991; c) D. W. Zhang, C. H. Chen, J. Zhang, F. Ren, *Chem. Mater.* **2005**, *17*, 5242.
[15] a) Z. Zeng, Z. Yin, X. Huang, H. Li, Q. He, G. Lu, F. Boey, H. Zhang, *Angew. Chem. Int. Ed.* **2011**, *50*, 11093; b) Z. Zeng, T. Sun, J. Zhu, X. Huang, Z. Yin, G. Lu, Z. Fan, Q. Yan, H. H. Hng, H. Zhang, *Angew. Chem. Int. Ed.* **2012**, *51*, 9052; c) T. Liu, Y. Ling, Y. Yang, L. Finn, E. Collazo, T. Zhai, Y. Tong, Y. Li, *Nano Energy* **2015**, *12*, 169.
[16] W. Chen, D. Deng, *Chem. Commun.* **2014**, *50*, 13327.
[17] J. Zhu, K. Y. S. Ng, D. Deng, *Cryst. Growth Design* **2014**, *14*, 2811.
[18] J. S. Chen, X. Chen, Y. Li, X. Chen, R. V. Ramanujan, X. Hu, *RSC Adv.* **2014**, *4*, 593.
[19] L. Li, G. Zhou, Z. Weng, X.-Y. Shan, F. Li, H.-M. Cheng, *Carbon* **2014**, *67*, 500.
[20] a) T. Yamashita, P. Hayes, *Appl. Surf. Sci.* **2008**, *254*, 2441; b) J. Liu, H. Cao, J. Xiong, Z. Cheng, *CrystEngComm* **2012**, *14*, 5140; c) X. Yao, C. Tang, G. Yuan, P. Cui, X. Xu, Z. Liu, *Electrochem. Commun.* **2011**, *13*, 1439; d) X. Zhang, Y. Chen, H. Liu, Y. Wei, W. Wei, *CrystEngComm* **2013**, *15*, 6184.
[21] a) W.-J. Yu, P.-X. Hou, F. Li, C. Liu, *J. Mater. Chem.* **2012**, *22*, 13756; b) Y. Luo, J. Luo, J. Jiang, W. Zhou, H. Yang, X. Qi, H. Zhang, H. J. Fan, D. Y. W. Yu, C. M. Li, T. Yu, *Energy Environ. Sci.* **2012**, *5*, 6559.
[22] a) L. Zhang, H. B. Wu, S. Madhavi, H. H. Hng, X. W. Lou, *J. Am. Chem. Soc.* **2012**, *134*, 17388; b) L. Zhang, H. B. Wu, R. Xu, X. W. Lou, *CrystEngComm* **2013**, *15*, 9332.
[23] a) D. Larcher, C. Masquelier, D. Bonnin, Y. Chabre, V. Masson, J.-B. Leriche, J.-M. Tarascon, *J. Electrochem. Soc.* **2003**, *150*, A133; b) D. Larcher, D. Bonnin, R. Cortes, I. Rivals, L. Personnaz, J.-M. Tarascon, *J. Electrochem. Soc.* **2003**, *150*, A1643; c) Z. Wang, D. Luan, S. Madhavi, Y. Hu, X. W. Lou, *Energy Environ. Sci.* **2012**, *5*, 5252.
[24] Q. Su, D. Xie, J. Zhang, G. Du, B. Xu, *ACS Nano* **2013**, *7*, 9115.
[25] J. Ma, J. Lian, X. Duan, X. Liu, W. Zheng, *J. Phys. Chem. C* **2010**, *114*, 10671.
[26] a) Y. Xu, G. Zhang, G. Du, Y. Sun, D. Gao, *Mater. Lett.* **2013**, *92*, 321; b) W.-W. Wang, Y.-J. Zhu, M.-L. Ruan, *J. Nanoparticle Res.* **2007**, *9*, 419; c) L.-P. Zhu, H.-M. Xiao, S.-Y. Fu, *Cryst. Growth Design* **2007**, *7*, 177.